

PARCEL: Physics-based unsupervised contrastive representation learning for parallel MR imaging

Shanshan Wang, *Senior Member, IEEE*, Ruoyou Wu, Cheng Li, *Senior Member, IEEE*, Juan Zou, Xin Liu, Qiegen Liu, Yan Xi, Hairong Zheng, *Senior Member, IEEE*

Abstract—With the successful application of deep learning to magnetic resonance (MR) imaging, parallel imaging techniques based on neural networks have attracted wide attention. However, in the absence of high-quality, fully sampled datasets for training, the performance of these methods is limited. To address this issue, this paper proposes a Physics-bAsed unsupeRvised Contrastive rEpresentation Learning (PARCEL) method to speed up parallel MR imaging. Specifically, PARCEL has a parallel framework to contrastively learn two branches of model-based unrolling networks directly from augmented undersampled k-space data. A sophisticated co-training loss with three essential components has been designed to guide the two networks in capturing the inherent features and representations for MR images. And the final MR image is reconstructed with the trained contrastive networks. PARCEL was evaluated on in vivo datasets and compared to five state-of-the-art methods. The results show that PARCEL is able to learn useful representations for more accurate MR reconstructions without relying on fully sampled datasets. The code will be made available at <https://github.com/ternencewu123/PARCEL>.

Index Terms—Deep learning, parallel imaging, contrastive representation learning, magnetic resonance imaging (MRI).

I. INTRODUCTION

PARALLEL imaging is an essential technique for accelerating MR imaging [1]-[3]. It utilizes magnetic resonance physics and the sensitivity of multiple coils to

reconstruct MR images from multi-coil measurements either directly in the k-space domain [1] or in the spatial domain [2]. The acceleration factor in classical parallel imaging is limited and its performance suffers from noise amplification effect [4]. To address this issue, compressed sensing along with different sparse prior knowledges have been introduced into parallel MR imaging, which can better remove aliasing artifacts and suppress noise [5]-[7]. However, it is difficult to determine the weight of regularization terms in compressed sensing methods, and its inherent iterative reconstruction process is very time-consuming [8]-[10].

To further promote MR imaging speed and automate weight parameter setting, deep learning has been introduced to MR reconstruction from undersampled data. These methods can be roughly divided into pure data-driven and model-based methods [10]. Pure data-driven methods require a neural network model to learn the mapping between artifact images and no-artifact images or undersampled k-space data and fully sampled k-space data [11]-[14]. Model-based methods based on the compressed sensing reconstruction algorithm unroll the iterative optimization process into a deep network, and use data training to learn parameters [15]-[18]. Generally, the model-based methods have better physical interpretability and is more robust compared to pure data-driven methods [10]. For example, Yang *et al.* [9] proposed a deep learning method called ADMM-CSNET that combined the traditional model-based method and data-driven deep learning method with the unrolled alternating direction method of multipliers (ADMM) process. Hammernik

This research was partly supported by Scientific and Technical Innovation 2030 - “New Generation Artificial Intelligence” Project (2020AAA0104100, 2020AAA0104105), the National Natural Science Foundation of China (61871371, 81830056), Key Laboratory for Magnetic Resonance and Multimodality Imaging of Guangdong Province (2020B1212060051), the Basic Research Program of Shenzhen (JCYJ20180507182400762), Youth Innovation Promotion Association Program of Chinese Academy of Sciences (2019351). (Corresponding author: Hairong Zheng, Shanshan Wang.)

Shanshan Wang is with the Paul C. Lauterbur Research Center for Biomedical Imaging, Shenzhen Institutes of Advanced Technology, Chinese Academy of Sciences, Shenzhen 518055, China and the Peng Cheng Laboratory, Shenzhen 518055, China (e-mail: ss.wang@siat.ac.cn; sophiasswang@hotmail.com).

Ruoyou Wu is with the Paul C. Lauterbur Research Center for Biomedical Imaging, Shenzhen Institutes of Advanced Technology, Chinese Academy of Sciences, Shenzhen 518055, China, the University of Chinese Academy of Sciences, Beijing 100049, China, and the Peng Cheng Laboratory, Shenzhen 518055, China (e-mail: ry.wu@siat.ac.cn).

Juan Zou is with the School of Physics and Optoelectronics, Xiangtan University, Xiangtan 411105, China, and the Paul C. Lauterbur Research Center for Biomedical Imaging, Shenzhen Institutes of Advanced Technology, Chinese Academy of Sciences, Shenzhen 518055, China (e-mail: zjuan@xtu.edu.cn).

Qiegen Liu is with the Department of Electronic Information Engineering, Nanchang University, Nanchang 330031, China. (e-mail: liuqiegen@ncu.edu.cn)

Cheng Li, Xin Liu, Yan Xi, and Hairong Zheng are with the Paul C. Lauterbur Research Center for Biomedical Imaging, Shenzhen Institutes of Advanced Technology, Chinese Academy of Sciences, Shenzhen 518055, China (e-mail: cheng.li6@siat.ac.cn; xin.liu@siat.ac.cn; y.xi@siat.ac.cn; hr.zheng@siat.ac.cn).

Shanshan Wang and Ruoyou Wu contributed equally to this manuscript.

et al. [8] combined the variational model with deep learning and embedded compressed sensing reconstruction into the gradient descent method to achieve the rapid reconstruction of MRI images. In addition, Aggarwal *et al.* [17] proposed MoDL, which uses a deep neural network as a regularization term and the conjugate gradient algorithm to solve the inverse problem in combination with data consistency.

The above methods have enabled great progress in accelerating MR imaging. However, they rely heavily on high quality, fully sampled MR images [18]. To decrease dependence on full reference data, self-supervised learning has been introduced for MRI [19]-[23]. Especially, Yaman *et al.* [19] proposed a self-supervised learning method (SSDU) for physics-guided deep learning reconstruction that divides measured data into two disjoint subsets, one used for training and the other used for loss calculation. This inspired method introduces the training of neural networks without fully sampled reference data. However, the performance of the method has room for improvement as it only uses a single network learned from two sets of disjoint k-space data. They therefore further investigate more augmented k-space subsets for deep learning MR reconstruction [21]. These methods have made encouraging contributions in MRI society. Nevertheless, unsupervised learning for fast MR imaging remains inadequately investigated. Contrastive representation learning [24] is a widely known unsupervised co-training framework that is very effective for obtaining essential and accurate representations for target samples [23]. To induce higher reconstruction accuracy, we propose the physics-based unsupervised contrastive representation learning (PARCEL) method, which investigates and integrates the strengths of contrastive representation learning [24] and model-based deep learning MR reconstruction models [17]. Specifically, we make the following key contributions in this study:

1) This paper proposed a PARCEL imaging framework which introduces unsupervised contrastive representation learning into parallel MR imaging. It simultaneously learns two model-based unrolling networks from augmented k-space data and then uses them for the final accurate MRI reconstruction.

2) A sophisticated co-training loss with three essential components has been designed to guide the two networks in capturing the inherent features and representations for MR images. Specifically, it has the undersampled calibration loss, reconstructed calibration loss and contrastive representation loss.

3) We compare PARCEL to five state-of-the-art methods with different sampling masks. The results show that PARCEL achieves good results in both qualitative and quantitative evaluations, which closely approaches the results achieved by supervised learning methods. In addition, PARCEL achieves better reconstruction than existing self-supervised methods.

The remainder of this paper is organized as follows. Section II introduces parallel magnetic resonance imaging and a brief recap of MoDL. Section III introduces the proposed method PARCEL. Section IV summarizes the experimental details and results, and Section V concludes the paper.

II. PRELIMINARY

A. Compressed Sensing based Parallel MR imaging

In parallel MR imaging, multiple receiver coils are used to accelerate MR imaging. Specifically, for the i -th coil measurement, we have:

$$y_i = \Omega F(S_i x) + \varepsilon_i, \quad i = 1, 2, \dots, C \quad (1)$$

where $y_i \in \mathbb{C}^M$ represents the measured k-space measurement corresponding to the i -th coil, Ω indicates the sampling mask, $\varepsilon_i \in \mathbb{C}^M$ represents measurement noise, C represents the number of coils to be measured, F is the normalized Fourier transform, $x \in \mathbb{R}^N$ is the to be reconstructed image, and S_i represents the sensitivity map of the i -th coil. S_i can be estimated using the k-space region corresponding to low frequencies (also known as the autocalibration signal, or ACS), which is fully sampled. In this experiment, we use the ESPIRiT [25] algorithm to construct the sensitivity maps. When applying compressed sensing to parallel MR imaging, the minimization formula can be described as follows:

$$\hat{x} = \arg \min_x \frac{1}{2} \|Ax - y\|_2^2 + \lambda \mathfrak{R}(x) \quad (2)$$

where $A = \Omega FS$ represents the encoding matrix with the diagonal matrix, S denotes the stack of all the coil sensitivities $S = \text{diag}\{S_i\}$. The first term represents the data consistency term, $\mathfrak{R}(x)$ represents the regularization term and λ represents the regularization coefficient.

B. A Brief Recap of MoDL

In order to solve (2), the regularization term can be a denoising regularization. A typical example is MoDL proposed in [17], which attempts to solve the following optimization problem:

$$\hat{x} = \arg \min_x \frac{1}{2} \|Ax - y\|_2^2 + \lambda \|N_w(x)\|^2 \quad (3)$$

where λ represents a trainable regularization parameter and $N_w(x) = x - D_w(x)$ denotes a learned convolutional neural network (CNN) of noise and alias corresponding to the “denoised” version $D_w(x)$ of x . With the alternating minimization algorithm, the model was solved as the following iteration process

$$\begin{cases} z^k = D_w(x^k) \\ x^{k+1} = (A^H A + \lambda I)^{-1} (A^H y + \lambda z^k) \end{cases} \quad (4)$$

where k is the iteration number and z^k is the intermediate denoised version of the image x^k . This iteration process is unrolled into a fully supervised learning process, which has two main modules, namely the residual learning based denoiser module $z = D_w(x)$ and the data consistency module for updating the image x^k . Here, the data consistency constraint is

solved by conjugate gradient method. Fig. 1 shows the specific MoDL architecture. The CNN based denoiser block $D_w(x)$ is shown in Fig. 1(a) and the unrolled neural network architecture is shown in Fig. 1(b), whose weights at different iterations are shared.

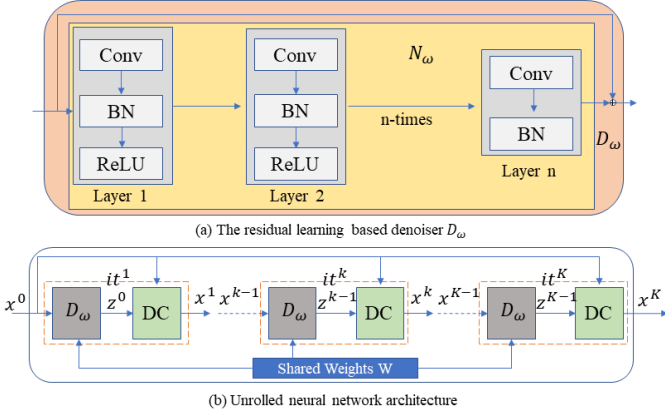


Fig. 1. The originally developed fully-supervised MoDL architecture. (a) shows the CNN based denoiser block $D_w(x)$. (b) is the unrolled architecture for K iterations. $D_w(x)$ share the weights across all the n iterations.

They used fully sampled datasets to train the regularization parameters and the unrolled neural network. The final image is generated as the output of the neural network.

III. THE PROPOSED METHOD

A. The Overall Framework of PARCEL

We proposed a physics-based unsupervised contrastive representation learning model PARCEL, whose overall framework is shown in Fig. 2. Its training phase has two branches of model-based networks unfolded with the conjugate gradient algorithm for solving the following formula:

$$\hat{x}_j = \arg \min_{x_j} \frac{1}{2} \|A_j x - y\|_2^2 + \lambda \|N_{w_j}(x)\|^2, j = 1, 2 \quad (5)$$

where $A_j = \Omega_j FS$. Specifically, the re-undersampled mask Ω_j ($j=1,2$ is the contrastive representation learning branch number), which needs to meet the following conditions: 1) two parallel networks sample different selection masks, 2) the input of the network contains mostly low-frequency signals and a small number of high-frequency signals, and 3) the number of selected data points is half the number of undersampled data points, namely

$$\begin{cases} \Omega_1 \neq \Omega_2 \\ \sum \Omega_j(\cdot) = \frac{1}{2} \sum \Omega(\cdot), j = 1, 2 \end{cases} \quad (6)$$

where $\sum \Omega(\cdot)$ denotes the total number of all sampling points. During the training phase, two re-undersampled masks Ω_1 and Ω_2 were used to perform secondary undersampling on the original undersampled data y to obtain y_1 and y_2 . The improved parallel MoDL model is used to train the data, and the

co-training loss function was specially designed to constrain the learning process of the model. During the testing phase, undersampled data are fed into the trained model to obtain reconstruction images x_1 and x_2 . Then the average of x_1 and x_2 is used as the final reconstruction result.

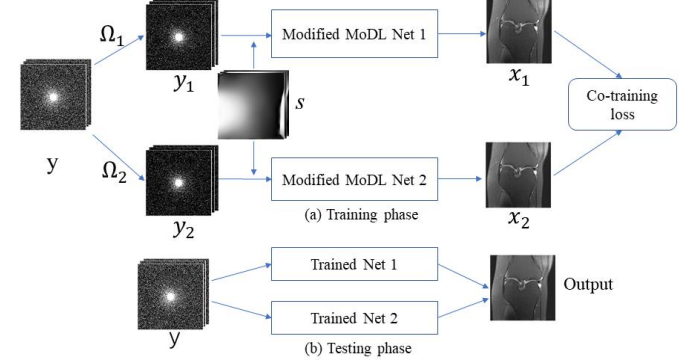


Fig. 2. The overall framework of PARCEL. (a) Training phase. Reundersampling is used to obtain two subsets y_1 and y_2 from the undersampled data y . Two reconstruction x_1 and x_2 are obtained through the trained parallel modified MoDL nets. The co-training loss is specially designed to constrain the contrastive learning process. (b) Testing phase. Undersampled data are fed into the trained model to obtain reconstruction images x_1 and x_2 . The average of x_1 and x_2 is used as the final reconstruction result.

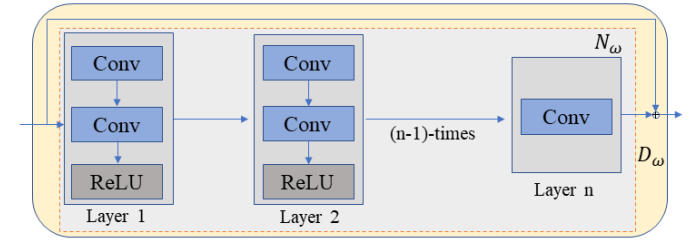


Fig. 3. The modified denoiser D_w . The batch normalization operation is replaced by the convolution operation, which is different from its original version as shown in Fig. 1(a).

B. The Modified-MoDL Architecture

Motivated by the fact that MoDL is very flexible and successful in fully-supervised deep learning, we adopted it as the backbone for our parallel training framework. But we have modified and adapted it to the self-supervised learning task. The original MoDL adopts batch normalization (BN) [26] for the residual learning denoiser. Its performance relies on the correct calculation of mean and variance of the datasets. Normally, the mean and variance of samples in the small batch are used to simulate the mean and variance of all data. However, BN trained with a small batch may suffer from bias or over-fitting issues. Therefore, it is not suitable for large-size MRI and direct deep learning from undersampled data. We have replaced it with the convolution operation. Compared with the BN, the continuous convolution operation can improve the denoising ability of the regularization term. As shown in Fig. 3, the whole module is based on two layers of convolution plus an activation function as the basic block. Then the basic block is cascaded with a convolution operation. The corresponding comparative experimental justification of this setting are presented in Section IV-F.

C. The Proposed Co-training Loss

We have designed a sophisticated co-training loss with three essential components to guide the two networks in capturing the inherent features and representations for MR images. Specifically, it has the undersampled calibration loss, reconstructed calibration loss and contrastive representation loss. Compared with self-supervised learning of a single network, contrastive learning of parallel networks allows for more rigorous and inherent features to be captured. In this way, the network is expected to avoid learning erroneous information. The mathematical formula of the total co-training loss function is as follows:

$$\begin{aligned} \xi_{ct}(x_1, x_2) = & \frac{1}{L} \left(\sum_{i=1}^N \ell_{uc}(Ax_1^i, y^i) + \sum_{i=1}^N \ell_{uc}(Ax_2^i, y^i) \right) \\ & + \frac{1}{L} \left(\sum_{i=1}^N \ell_{rc}(x_1^i) + \sum_{i=1}^N \ell_{rc}(x_2^i) \right) \\ & + \frac{1}{L} \sum_{i=1}^N \ell_{cl}(x_1^i, x_2^i) \end{aligned} \quad (7)$$

where L is the total number of training samples, i is the i -th training sample, ℓ_{ct} represent co-training loss. ℓ_{uc} represent undersampled calibration loss; ℓ_{rc} represent reconstructed calibration loss; ℓ_{cl} represent contrastive representation loss and x_1^i and x_2^i represent the outputs of the two networks respectively

1) Undersampled Calibration Loss: The undersampled calibration loss is mainly concerned with the k-space points that have been sampled, which ensures that the reconstruction results of the sampling elements are consistent with the zero-filled reconstructed image from the measurement. Specifically, the reconstructed images is under sampling with the encoding matrix and then inversed with Fourier transform. It was used to calculate the difference between the undersampled version of the network prediction and the directly zero-filled inverse one. The specific calculation formula is as follows:

$$\ell_{uc}(Ax, y) = \ell_{mse}(F^{-1}Ax, F^{-1}y) \quad (8)$$

where F^{-1} represents the two-dimensional inverse Fourier transform.

$$\ell_{mse}(a, b) = \frac{1}{N} \sum_{l=1}^N (a_l - b_l)^2 \quad (9)$$

where N represents size of the image. This operation is trying to calibrate the reconstructed images is consistent with the one directly inversed reconstructed from the sampled measurements.

2) Reconstructed Calibration Loss: The reconstructed calibration loss (obtained by applying an affine projection based on the undersampling mask) is constructed and applied to the outputs of the parallel networks, which not only ensures that the reconstruction results do not deviate from the

measurement results but also improves the signal-to-noise ratio of the reconstructed image [13], as shown in Fig. 4. Specifically, the reconstructed image is first transformed into k-space and multiplied with the inverse mask. Then the input undersampled data is added. The sum of the two is transformed into the image domain. Finally the mean square error is calculated with the reconstructed image. The specific calculation formula is as follows:

$$\ell_{rc}(x) = \ell_{mse}(x, (Fx(\mathbf{1} - \Omega) + y)F^{-1}) \quad (10)$$

where x represents the output of network 1 or network 2.

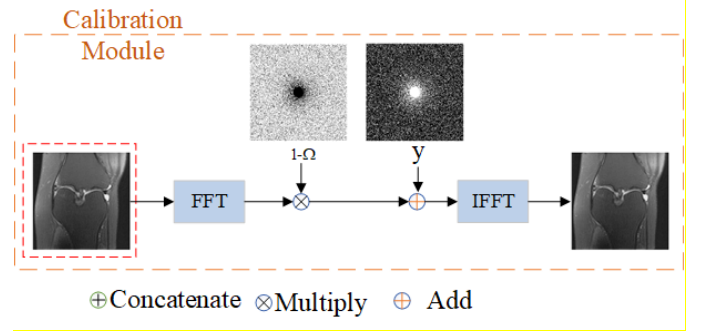


Fig. 4. The reconstructed calibration module.

3) Contrastive Representation Loss: We construct a contrastive representation loss based on contrastive representation learning, which can dig into deeper levels of similar information and detailed features, to ensure the outputs of the two networks are as consistent as possible. Data are expanded by generating different inputs through two transformations, and the inputs are encoded into features. Finally, the similarity of the two features is maximized to ensure that the outputs of the upper and lower networks are close enough. It is expected to more effectively recover high frequency information. The specific calculation formula is as follows:

$$\ell_{cl}(x_1, x_2) = -\log \frac{\exp(\text{sim}(x_1, x_2))}{\exp(\text{sim}(x_1, x_2)) + \gamma} \quad (11)$$

where $\text{sim}(x_1, x_2) = \frac{x_1^T x_2}{\|x_1\| \|x_2\|}$, T represent the transpose of the matrix, γ is a regulating parameter used to prevent the co-training loss from falling to 0 and $\text{sim}(x_1, x_2)$ is maximized by minimizing $\ell_{cl}(x_1, x_2)$ so that x_1 and x_2 are as close as possible.

IV. EXPERIMENTS AND RESULTS

A. Datasets

Knee data were obtained from the NYU fastMRI database [27] and approved by the NYU School of Medicine Institutional Review Board. Fully sampled MRI data were acquired on one of three clinical 3T systems (Siemens Magnetom Skyra, Prisma and Biograph mMR) or one clinical 1.5T system (Siemens Magnetom Aera). Data acquisition was achieved with a 15-

channel knee coil array and a conventional Cartesian 2D TSE protocol. The dataset includes data from two pulse sequences, yielding coronal proton-density weighting with (PD-FS) and without (PD) fat suppression. As per standard clinical protocol, the sequence parameters were matched as closely as possible between the two systems. The specific sequence parameters used were: echo train length 4, matrix size 320×320 , in-plane resolution $0.5 \text{ mm} \times 0.5 \text{ mm}$, slice thickness 3 mm, and no gap between slices. The timing varied from system to system, with a repetition time (TR) of between 2200 and 3000 ms, and an echo time (TE) between 27 and 34 mm. The shape of the k-space tensor is slices \times coils \times height \times weight. In this experiment, the train, verification and test sets contain 156, 37 and 52 volumes, respectively. In the experiment, both one and two-dimensional random undersampled masks were tested; the corresponding masks are shown in Fig. 5.

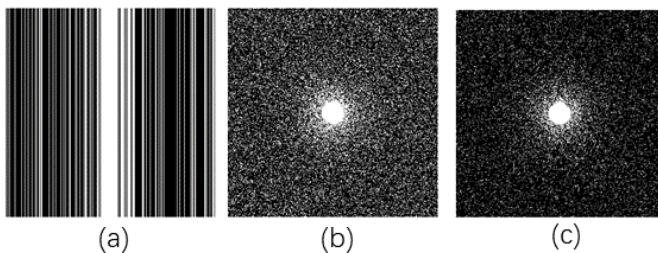


Fig. 5. Two types of sampling. (a) One-dimensional random undersampled mask with $R=3$. Two-dimensional random undersampled masks with (b) $R=4$ and (c) $R=8$. R represents the acceleration rate. The autocalibration signal (ACS) lines of the undersampled masks is 24.

B. Implementation Details

We use a deep neural network with 5 layers, each with 64 convolution kernels to achieve D_ω , and the size of the convolution kernel is 3×3 . Each layer contains two continuous convolution operations and a linear activation function, ReLU (rectified linear unit, $f(x) = \max(0, x)$). The last layer has only one convolution operation. We extract the output of block D_w to the data consistency layer. In the experiment, the specific layer number of D_w is 5, and the number of alternate iterations of network unfolding, K , is 5 [17]. The data consistency layer outputs complex values as well as inputs. Module D_w provides input by superimposing the real and imaginary parts in a channel. Among these, coil sensitivity is estimated from the central k-space region of each slice using the ESPIRiT [25] algorithm, with all assumptions known in the experiment. During training, we used ADAM [28] optimization, and the momentum was (0.9, 0.999). The initial rate was 10^{-4} , and the learning rate attenuation strategy was adopted [29]. The loss value of the verification set was taken as the monitoring indicator, and the learning rate was multiplied by 0.3 when the loss no longer decreased within 10 epoch periods. If the loss did not change within 50 epochs, the training ends. The total epoch was 200, and the batch size was 2. Parallel training was adopted. We train the network under two random masks and different acceleration factors to explore the reconstruction effect of the model under different sampling methods. The model is implemented in Pytorch and the source code can be downloaded

from this link: <https://github.com/ternencewu123/PARCEL>.

C. Evaluation Metrics

In the experiment, peak signal-to-noise ratio (PSNR) and structural similarity (SSIM) [30] were used to quantitatively evaluate the experimental results. The SSIM index is the product of the luminance, contrast and structure measure functions. We compared the proposed PARCEL, CSTV (compressed sensing with total variation), VarNet [8], U-Net-256, SSDU [19] and supervised-MoDL [17] methods under different acceleration rates and sampling modes.

D. Evaluation with Different Sampling Masks.

1) *2D Random Sampling*: We compared PARCEL with five methods, namely, CSTV, VarNet [8], U-Net-256, SSDU [19], and supervised-MoDL [17]. CSTV is a conventional PI-based method. VarNet, U-Net-256, and supervised-MoDL are trained using pairs of measurement data and ground truth images. VarNet learns variational networks to accelerate MRI reconstruction. U-Net-256 is a U-Net model trained in a supervised manner, where the number of channels of the last encoder layer is 256. SSDU is a model-based method in which an MoDL model trained in a self-supervised manner as in [19]. Supervised-MoDL is an MoDL model trained in a supervised manner. CSTV is implemented in Matlab (Math Works, Natick, MA), and the other methods are implemented in Python.

Fig. 6 demonstrates the reconstruction results of coronal PD images with acceleration rates of Fig. 6(a) $R=4$ and Fig. 6(b) $R=8$ using CSTV, VarNet, U-Net-256, SSDU, supervised-MoDL and the proposed unsupervised model PARCEL. The first row shows the reconstructed images, the second row represents local detail graphs of the reconstructed images, and the third row presents error maps between the reconstructed and the reference images. The CSTV, VarNet, and U-Net-256 approaches suffer from visible residual artifacts and do not recover detailed structure due to over-smoothing problems, as shown in the error maps. SSDU, supervised-MoDL, and our approach PARCEL successfully remove residual artifacts and recover detailed structure. Compared with SSDU, our method achieves better reconstruction results, and the model is more stable. This is mainly due to contrastive representation learning's ability to dig deep for information and co-training loss constrain on the network. Moreover, SSDU has worse reconstruction results at the acceleration rate of 8. Furthermore, the performance of our method is close to that of supervised-MoDL at the acceleration rate of 8 and may have benefited from the constraint of reconstructed calibration loss on reconstruction results to avoid deviation from the measured data. The quantitative metrics and error maps shown in Fig. 6 are consistent with these observations, and our method achieves good results at both acceleration rates.

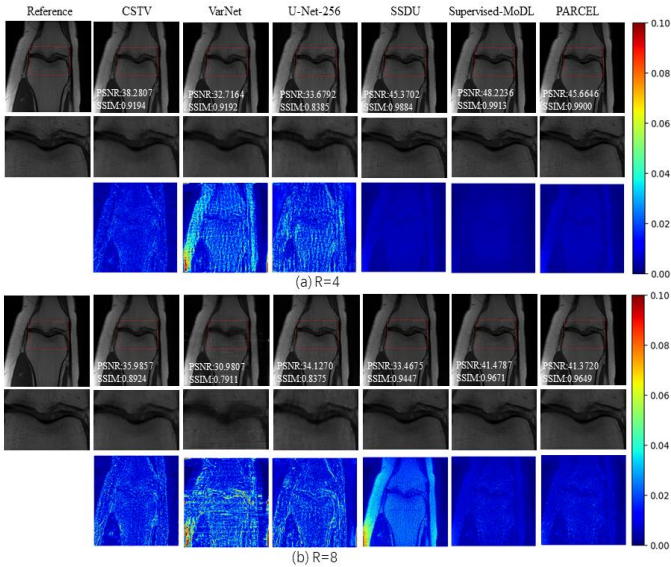


Fig. 6. Reconstruction results of an example test slice from the fastMRI coronal proton density (PD) knee MRI dataset with acceleration rates of $R=4$ (a) and $R=8$ (b). Fully sampled images are shown in the first column for reference. The remaining columns show the reconstructed images of CSTV, VarNet, U-Net-256, SSDU, supervised-MoDL and PARCEL. With the exception of the supervised-MoDL method, our proposed model PARCEL generates better results than the other methods.

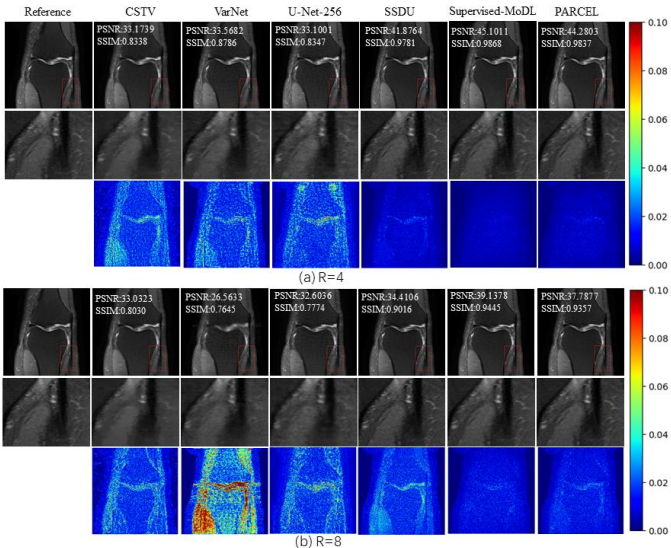


Fig. 7. Reconstruction results of an example test slice from the fastMRI coronal proton density weighted with fat suppression (PD-FS) dataset with acceleration rates of $R=4$ (a) and $R=8$ (b). Fully sampled images are shown in the first column for reference. The remaining columns show the reconstructed images of CSTV, VarNet, U-Net-256, SSDU, supervised-MoDL and PARCEL. With the exception of the supervised-MoDL method, our proposed model PARCEL shows better results than the other methods.

Similar results can be observed for coronal PD-FS images with acceleration rates of $R=4$ (a) and $R=8$ (b), as depicted in Fig. 7. PARCEL and supervised-MoDL achieve similar performance while improving the suppression of the residual artifacts visible in VarNet and U-Net-256. The quantitative evaluation results as well as the residual artifacts in the error maps also highlight these observations. With an increase in acceleration rate, our method can also achieve improved reconstruction results. However, compared with coronal PD-FS

images, the reconstruction quality of coronal PD images increases overall.

Fig. 8 and Fig. 9 show box plots displaying the median and interquartile range (25th-75th percentile) of the quantitative metrics for PSNR and SSIM with acceleration rates of $R=4$ and $R=8$, across all test data sets for each knee sequence. For all sequences, PARCEL and supervised-MoDL achieve similar quantitative performance for both PSNR and SSIM, significantly outperforming CSTV, VarNet and U-Net-256. In particular, for the SSIM metric, the results of the values taken are relatively concentrated, which indicates good generalization and highlights the excellent performance of our model.

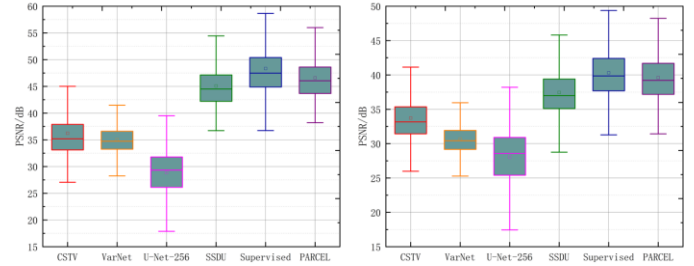


Fig. 8. Box plots showing the median and interquartile range (25th-75th percentile) of PSNR calculated using the test data. Our proposed unsupervised method PARCEL, supervised-MoDL (represented by the Supervised in the diagram), and SSDU give higher PSNR values than CSTV, VarNet and U-Net-256, and our method generates results very close to supervised-MoDL, which is a fully supervised method.

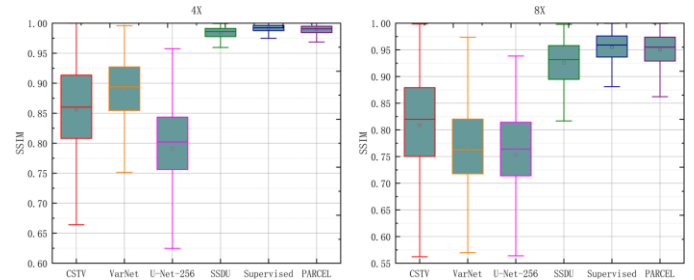


Fig. 9. Box plots showing the median and interquartile range (25th-75th percentile) of SSIM calculated using the test data. Our proposed unsupervised method PARCEL, supervised-MoDL (represented by the Supervised in the diagram), and SSDU give higher SSIM values than CSTV, VarNet, and U-Net-256, and our method generates results very close to supervised-MoDL, which is a fully supervised method.

2) 1D Random Sampling: To further evaluate model reconstruction quality, we continued our experiments using a one-dimensional random mask. Fig. 10 show the results for evaluation indicators PSNR and SSIM, respectively. Additionally, Fig. 11 and Fig. 12 show representative reconstructions of the knee test set using various reconstruction methods at the acceleration rates (3x) along with their error maps using a jet color map (blue: low, red: high error). These experimental results show that PARCEL is able to reconstruct the images with improved PSNR and SSIM. The error map clearly shows that SSDU, supervised-MoDL and PARCEL maintain detailed information better than the other methods. The pure U-Net network fails to achieve good result. however, it is effective in realizing the reconstruction ability of the MRI image domain. In addition, our method achieves good reconstruction results under high acceleration rates with reconstruction results close to those of supervised learning. The

experimental observations using a one-dimensional random mask is similar to the those obtained by using a two-dimensional random mask. The two and one-dimensional experimental results indicate that two-dimensional random mask reconstruction achieves the best performance. For example, two-dimensional random masks with acceleration rates of 4 outperform one-dimensional random masks with acceleration rates of 3. These experimental results are obtained from a comparison between Fig. 6 and Fig. 11. Moreover, the two-dimensional random mask with the acceleration rates of 4 performs better than the one-dimensional random mask with the acceleration rates of 3 on fat suppression data, as shown in Fig. 7 and Fig. 12. Compared with one-dimensional sampling, two-dimensional Poisson sampling is more effective for sampling the high frequency region.

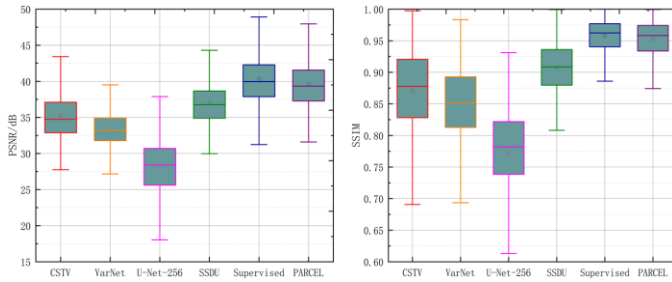


Fig. 10. Box plots showing the median and interquartile range (25th-75th percentile) of PSNR and SSIM calculated using the test data with the acceleration rates of $R = 3$. Our proposed unsupervised method PARCEL, supervised-MoDL (represented by the Supervised in the diagram), and SSDU give higher PSNR and SSIM values than CSTV, VarNet and U-Net-256, and our method generates results very close to supervised-MoDL, which is a fully supervised method.

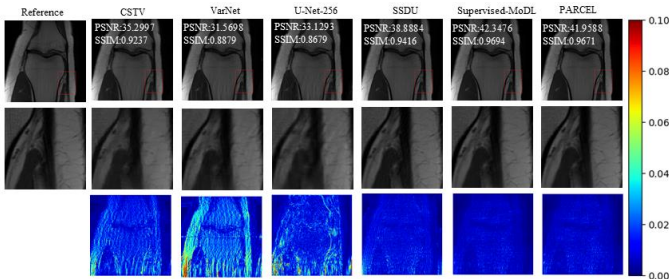


Fig. 11. Reconstruction results of an example test slice from the fastMRI coronal proton density (PD) knee MRI dataset with the acceleration rates of $R = 3$. Fully sampled images are shown in the first column for reference. The remaining columns show the reconstructed images of CSTV, VarNet, U-Net-256, SSDU, supervised-MoDL and PARCEL. With the exception of the supervised-MoDL method, our proposed model PARCEL shows better results than the other methods.

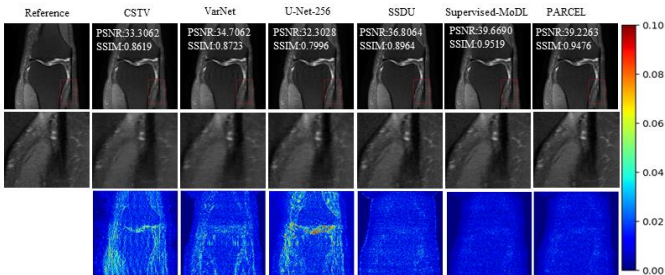


Fig. 12. Reconstruction results of an example test slice from the fastMRI coronal density weighted with fat suppression (PD-FS) dataset with the

acceleration rates of $R=3$. Fully sampled images are shown in the first column for reference. The remaining columns show the reconstructed images of CSTV, VarNet, U-Net-256, SSDU, supervised-MoDL and PARCEL. With the exception of the supervised-MoDL method, our proposed model PARCEL shows better results than the other methods.

E. Validation of Contrastive Representation Learning.

To evaluate the effects of contrastive representation learning, we conducted experiments about contrastive representation loss under two-dimensional random masks. Fig. 13 and Fig. 14 show a quantitative comparison of the contrastive representation loss. The parallel network is more efficient for MRI reconstruction when the acceleration rate is increased. The PSNR index increased from 0.3755 dB at the acceleration rate of 4 to 1.7735 dB at the acceleration rate of 8 in Fig. 13. Fig. 15 and Fig. 16 represent the qualitative evaluation results of the contrastive representation loss about Single-Net, Parallel-Net, CL (a PARCEL model with undersampled calibration and contrastive representation loss), and supervised-MoDL, respectively. While Single-Net is an end-to-end self-supervised MoDL model, Parallel-Net is a PARCEL model with undersampled calibration loss only. Compared with traditional self-supervised learning methods, such as Single-Net, the reconstructed images are improved in terms of quantitative metrics by using a contrastive representation learning approach with parallel networks. For example, the PSNR metric improves from 41.4001 dB to 43.0034 dB at the acceleration rate of 4 in Fig. 15(a). It is evident that contrastive representation learning improves the quality of the reconstructed images. Moreover, we also compare the difference between the two outputs of the parallel network before and after the inclusion of the contrastive representation loss, and the results are shown in Table I. According to the experimental results, after the inclusion of the contrastive representation loss, the difference between the two output results of the parallel network is smaller, indicating that the two outputs results are closer. This is largely due to the ability of contrastive representation learning to mine deep information by learning the internal similarities between two re-undersampled data from the same undersampled k -space, thus ensuring that the information learned by the two networks is as similar as possible.

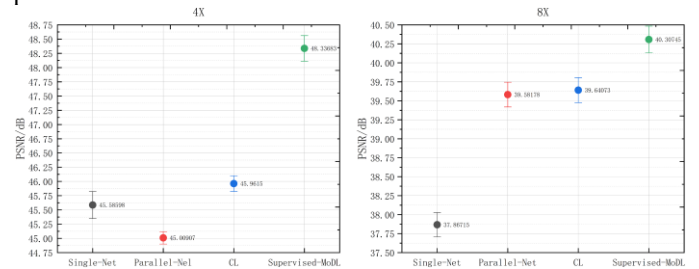


Fig. 13. Quantitative comparison of contrastive representation loss in PSNR. The bullseyes show the means, and the error bars show the errors on the means.

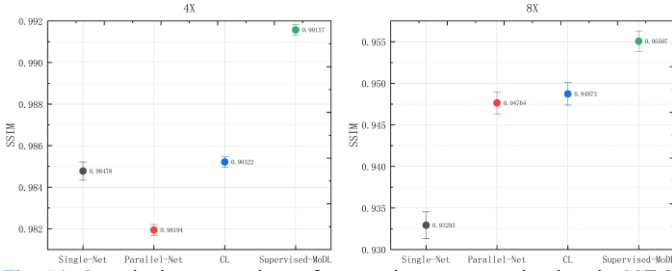


Fig. 14. Quantitative comparison of contrastive representation loss in SSIM. The bullseyes show the means, and the error bars show the errors on the means.

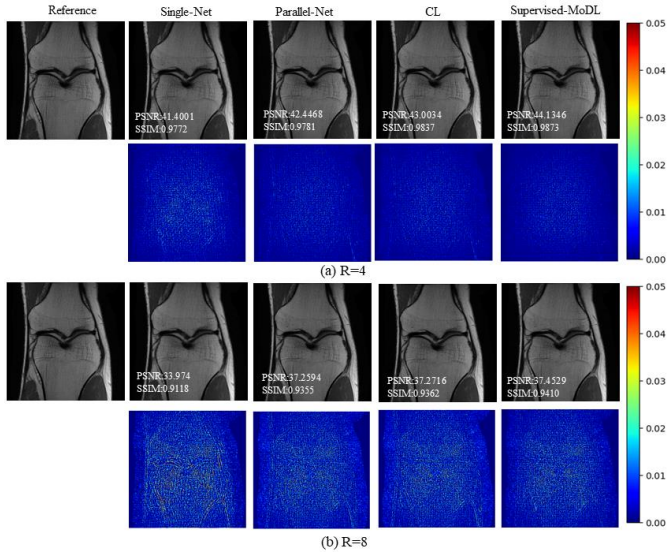


Fig. 15. Reconstruction results of an example test slice from the fastMRI coronal proton density (PD) knee MRI dataset with the acceleration rates of R=4 (a) and R=8 (b). Fully sampled images are shown in the first column for reference. The remaining columns show the reconstructed images of Single-Net (solely consists of a single MoDL network), Parallel-Net (has the same structure as our network, but contains only undersampled calibration loss), CL (a PARCEL model with undersampled calibration and contrastive representation loss), and supervised-MoDL.

F. Ablation Study.

In Section III-B, we made changes to the D_w module. The BN [26] operation in the original literature [17] was replaced by a convolution operation. We compared the differences between the two denoising modules, and the results are shown in Table II. Compared with BN, the convolution operation considerably improves the evaluation index. This is mainly due to the small batch of data cannot go on to estimate all the data, resulting in poor generalization of the model. This improvement associated with the convolution operation becomes clearer with increased acceleration rate.

Table I

QUANTITATIVE COMPARISON RESULTS OF PARALLEL NETWORK OUTPUTS WITHOUT $\ell_{cl}(o)$ AND WITH $\ell_{cl}(w)$ THE CONTRASTIVE LOSS

Acceleration rate	Method	PSNR/dB	SSIM
R=4	$\ell_{cl}(o)$	52.6289 ± 3.7630	0.9972 ± 0.0021
		53.8485 ± 3.1481	0.9973 ± 0.0018
	$\ell_{cl}(w)$	52.6289 ± 3.7630	0.9972 ± 0.0021
		53.8485 ± 3.1481	0.9973 ± 0.0018

R=8	$\ell_{cl}(o)$	50.8849 ± 2.6404	0.9969 ± 0.0010
	$\ell_{cl}(w)$	51.2117 ± 2.9009	0.9972 ± 0.0011

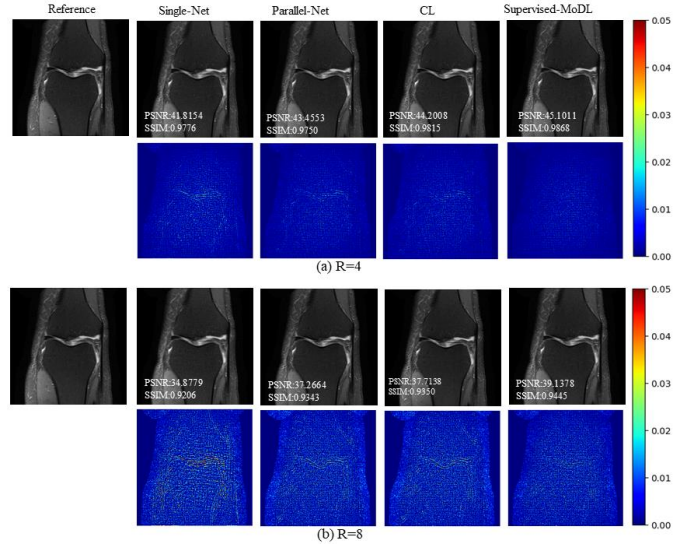


Fig. 16. Reconstruction results of an example test slice from the fastMRI coronal proton density weighted with fat suppression (PD-FS) knee MRI dataset with the acceleration rates of R=4 (a) and R=8 (b). Fully sampled images are shown in the first column for reference. The remaining columns show the reconstructed images of Single-Net (solely consists of a single MoDL network), Parallel-Net (has the same structure as our network, but contains only undersampled calibration loss), CL (a PARCEL model with undersampled calibration and contrastive representation loss), and supervised-MoDL.

Table II

COMPARISON OF EXPERIMENTAL RESULTS OF THE BN AND CONV OPERATION

Acceleration rate	Method	PSNR/dB	SSIM
R=4	BN(w)	45.2425 ± 4.5054	0.9845 ± 0.0097
	Conv(w)	46.5860 ± 4.2046	0.9893 ± 0.0070
R=8	BN(w)	36.1758 ± 2.6977	0.9109 ± 0.0379
	Conv(w)	39.6025 ± 3.6589	0.9501 ± 0.0303

To evaluate the different loss functions proposed, relevant experiments were carried out. Table III shows the results of ablation studies conducted with different loss functions. Among these, the calculation formula of contrastive representation loss is shown in (11), and the calculation formula of reconstructed calibration loss is shown in (10). The loss of contrastive representation loss was previously discussed. Here, we mainly discuss the reconstructed calibration loss and the combination between reconstructed calibration loss and contrastive representation loss. The ablation experimental results are based on a two-dimensional random mask. Regarding reconstructed calibration loss at the acceleration rates of 4 and 8, the PSNR value increased by 0.9695 dB and 1.74 dB, respectively, compared with Single-Net. Similarly, regarding the combination between reconstructed calibration loss and contrastive representation loss, the PSNR value increased by 0.9965 dB and 1.7736 dB, respectively, compared with Single-Net. In the ablation experiment, this improvement in reconstruction performance is more apparent at high

acceleration rates. When the acceleration rate is 4 and 8, the combination between reconstruction calibration loss and contrastive representation loss achieves the best result. In general, the reconstruction calibration loss between parallel networks can further improve the reconstruction performance of the model. In addition, the ability of contrastive representation learning to extract deep information improves the reconstruction effect.

The experimental results show that, on both the PSNR and SSIM indicators, the MRI reconstruction model constructed by unsupervised contrastive representation learning outperforms the classical compressed sensing algorithm and a newly proposed self-supervised method [19] with improved model stability while gradually approaching the performance of the supervised method. Our PARCEL model is constructed based on an iterative network of theoretical derivation, which provides mathematical rigor for MRI reconstruction, making the approach both theoretically and practically attractive. Moreover, having a network based on iterative unfolded networks solves the problem of traditional pure neural networks having too many parameters. Compared with pure the neural network model, the iteratively unfolded network achieves better results per the comparison between the U-Net-256 and PARCEL models shown in Fig. 6 and Fig. 7.

In this study, we used a 9-layer convolutional neural network to realize the denoising module, as shown in Fig. 3. This part of the neural network has no fixed requirements, but can utilize the classical U-Net network. The reconstruction results might be improved by using more complex network structures. In

addition, the sharing of network parameters allows the network to perform a greater number of iterations without increasing the number of parameters. Other optimization methods, such as ISTA [31], can be employed to solve the optimization problem in (3). In addition, from the experiments in Section IV-D, we conclude that two-dimensional random masks (which benefit from effective sampling of high-frequency information) are better than one-dimensional random masks. In future work, we will try new optimization methods to solve the optimization problems in (3) and explore a greater number of sample patterns.

V. CONCLUSION

In this paper, we propose a physics-based unsupervised contrastive representation learning method to speed up parallel MR imaging. It has a parallel framework to contrastively learn two branches of model-based unrolling networks directly from augmented undersampled k-space data. To guide the two networks in capturing the inherent features and representations for MR images, a sophisticated co-training loss with three essential components has been designed. Finally, the final MR image is reconstructed with the trained contrastive networks. PARCEL was evaluated on in vivo datasets and compared to five state-of-the-art methods. The results show that PARCEL is able to learn useful representations for more accurate MR reconstructions without relying on fully sampled datasets. In the future we will investigate contrastive representation learning for dynamic or multi-contrast MR imaging. Our code is available at <https://github.com/ternencewu123/PARCEL>.

Table III

QUANTITATIVE COMPARISON OF RECONSTRUCTED MAGNETIC RESONANCE IMAGING USING PARCEL WITH THE DIFFERENT LOEESSE AND TWO BASELINE MODEL WITH TWO ACCELERATION RATE (MEAN \pm STD)

Acceleration rate	Model	PSNR/dB	SSIM
R=4	Single-Net	45.5895 \pm 5.2523	0.9847 \pm 0.0096
	Parallel-Net ℓ_{uc}	45.0090 \pm 2.4028	0.9819 \pm 0.0059
	Parallel-Net $\ell_{uc} + \ell_{cl}$	45.9615 \pm 3.0238	0.9852 \pm 0.0055
	Parallel-Net $\ell_{uc} + \ell_{rc}$	46.5590 \pm 4.2367	0.9891 \pm 0.0072
	Parallel-Net $\ell_{uc} + \ell_{cl} + \ell_{rc}$	46.5860 \pm 4.2046	0.9893 \pm 0.0070
R=8	Single-Net	37.8671 \pm 3.5245	0.9329 \pm 0.0353
	Parallel-Net ℓ_{uc}	39.5817 \pm 3.5850	0.9476 \pm 0.0291
	Parallel-Net $\ell_{uc} + \ell_{cl}$	39.6025 \pm 3.6589	0.9487 \pm 0.0296
	Parallel-Net $\ell_{uc} + \ell_{rc}$	39.6071 \pm 3.6558	0.9499 \pm 0.0301
	Parallel-Net $\ell_{uc} + \ell_{cl} + \ell_{rc}$	39.6407 \pm 3.6367	0.9501 \pm 0.0303

REFERENCES

- [1] M. A. Griswold, P.M. Jakob, R.M. Heidemann, M. Nittka, V. Jellus, J. M. Wang, B. Kiefer, A. Haase, "Generalized autocalibrating partially parallel acquisitions (GRAPPA)," *Magnetic Resonance in Medicine.*, vol. 47, no. 6, pp. 1202-1210, 2002.
- [2] K. P. Pruessmann, M. Weiger, M. B. Scheidegger, P. Boesiger, "SENSE: sensitivity encoding for fast MRI," *Magnetic Resonance in Medicine.*, vol. 42, no. 5, pp. 952-962, 1999.
- [3] D. K. Sodickson and W. J. Manning, "Simultaneous acquisition of spatial harmonics (SMASH): fast imaging with radiofrequency coil arrays," *Magnetic Resonance in Medicine.*, vol. 38, no. 4, pp. 591-603, 1997.
- [4] P. M. Robson, A. K. Grant, A. J. Madhuranthakam, R. Lattanzi, D. K. Sodickson, C. A. McKenzie, "Comprehensive quantification of signal-to-noise ratio and g-factor for image-based and k-space-based parallel imaging reconstructions," *Magnetic Resonance in Medicine.*, vol. 60, no. 4, pp. 895-907, 2008.
- [5] S. Wang, S. Tan, Y. Gao, et al., "Learning Joint-Sparse Codes for Calibration-Free Parallel MR Imaging," in *IEEE Transactions on Medical Imaging*, vol. 37, no. 1, pp. 251-261, Jan. 2018
- [6] M. Lustig, J. M. Pauly, "Spirit: iterative self-consistent parallel imaging reconstruction from arbitrary k-space," *Magnetic Resonance in Medicine.*, vol. 64, no. 2, pp. 457-471, 2010.
- [7] K. H. Jin, D. Lee, J. C. Ye, "A general framework for compressed sensing and parallel MRI using annihilating filter based low-rank Hankel matrix," *IEEE trans. Computat. Imag.*, vol. 2, no. 4, pp. 480-495, 2016.

- [8] K. Hammernik, T. Klatzer, E. Kobler, M. P. Recht, D. K. Sodickson, T. Pock, F. Knoll, "Learning a variational network for reconstruction of accelerated MRI data," *Magnetic Resonance in Medicine.*, vol. 79, no. 6, pp. 3055-3071, 2018.
- [9] Y. Yang, Sun, H. B. Li, Z. B. Xu, "ADMM-CSNet: A deep learning approach for image compressive sensing," *IEEE Transactions on Pattern Analysis and Machine Intelligence.*, vol. 42, no. 3, pp. 521-538, 2020.
- [10] Wang SS, Xiao TH, Liu QG, Zheng HR. Deep learning for fast MR imaging: a review for learning reconstruction from incomplete k-space data. *Biomedical Signal Processing Control.* 2021; 68: 102579
- [11] S. Wang et al., "Accelerating magnetic resonance imaging via deep learning", *Proc. IEEE 13th Int. Symp. Biomed. Imag. (ISBI)*, pp. 514-517, Apr. 2016.
- [12] D. Lee, J. Yoo, S. Tak, J. C. Ye, "Deep residual learning for accelerated MRI using magnetic and phase networks," *IEEE Transactions on Biomedical Engineering.*, vol. 64, no. 9, pp. 1985-1995, 2018.
- [13] M. Mardani, E. Gong, J. Y. Cheng, S. S. Vasanawala, G. Zaharchuk, L. Xing, J. M. Pauly, "Deep generative adversarial neural networks for compressive sensing MRI." *IEEE Transactions on Medical Imaging.*, vol. 38, no. 1, pp. 167-179, 2019.
- [14] M. Akçakaya, S. Moeller, S. Weingärtner, K. Uğurbil, "Scan-specific robust artificial-neural-networks for k-space interpolation (RAKI) reconstruction: Database-free deep learning for fast imaging," *Magnetic Resonance in Medicine.*, vol. 81, no. 1, pp. 439-453, 2018.
- [15] J. Schlemper, J. Caballero, J. V. Hajnal, A. N. Price, D. Rueckert, "A deep cascade of convolutional neural networks for dynamic MR image reconstruction," *IEEE Transactions on Medical Imaging.*, vol. 37, no. 2, pp. 491-503, 2017.
- [16] J. Zhang, B. Ghanem, "ISTA-Net: Interpretable optimization-inspired deep network for image compressive sensing," In: *Proceedings of the IEEE Conference on Computer Vision and Pattern Recognition*, Salt Lake City, Utah, 2018, pp. 1828-1837.
- [17] H. K. Aggarwal, M. P. Mani, M. Jacob, "MoDL: Model-based deep learning architecture for inverse problems," *IEEE Transactions on Medical Imaging.*, vol. 38, no. 2, pp. 394-405, 2019.
- [18] F. Knoll, K. Hammernik, C. Zhang, S. Moeller, T. Pock, D.K. Sodickson, M. Akçakaya, "Deep-Learning Methods for parallel magnetic resonance imaging reconstruction: a survey of the current approaches, trends, and issues." *IEEE Signal Processing Magazine.*, vol. 37, no. 1, pp. 128-140, 2020.
- [19] B. Yaman, S. A. H. Hosseini, S. Moeller, J. Ellermann, K. Uğurbil, M. Akçakaya, "Self-supervised learning of physics-guided reconstruction neural networks without fully sampled reference data," *Magnetic Resonance in Medicine.*, vol. 84, no. 6, pp. 3172-3191, 2020.
- [20] F. Liu, R. Kijowski, G. El Fakhri, L. Feng, "Magnetic resonance parameter mapping using model-guided self-supervised deep learning," *Magnetic Resonance in Medicine.*, vol. 85, no. 6, pp. 3211-3226, 2021.
- [21] B. Yaman, S. A. H. Hosseini, S. Moeller, J. Ellermann, K. Uğurbil, M. Akçakaya, "Ground-truth free multi-mask self-supervised physics-guided deep learning in highly accelerated MRI," *2021 18th international Symposium on Biomedical Imaging (ISBI)*, Nice, France, 2021, pp. 1850-1854.
- [22] W. J. Gan, Y. Y. Hu, C. Eldeniz, J. M. Liu, Y. S. Chen, H. Y. An, U. S. Kamilov, "SS-JIRCS: self-supervised joint image reconstruction and coil sensitivity calibration in parallel MRI without ground truth," *Proceedings of the IEEE/CVF International Conference on Computer Vision*, 2021, pp. 4048-4056.
- [23] C. Hu, C. Li, H. F. Wang, Q. G. Liu, H. R. Zheng, S. S. Wang, "Self-supervised learning for MRI reconstruction with a parallel network training framework." *International Conference on Medical Image Computing and Computer-Assisted Intervention*, Springer, Cham, 2021, pp. 382-391.
- [24] T. Chen, S. Kornblith, M. Norouzi, G. Hinton, "A simple framework for contrastive learning of visual representation," *International Conference on Machine Learning, PMLR*, 2020, pp. 1597-1607.
- [25] M. Uecker, P. Lai, M. J. Murphy, P. Virtue, M. Elad, J. M. Pauly, S. S. Vasanawala, M. Lustig, "ESPIRiT-an eigenvalue approach to autocalibrating parallel MRI: Where SENSE meets GRAPPA," *Magnetic Resonance in Medicine.*, vol. 71, no. 3, pp. 990-1001, 2014.
- [26] S. Ioffe, C. Szegedy, "Batch normalization: Accelerating deep network training by reducing internal covariate shift," *International Conference on Machine Learning, PMLR*, 2015, pp. 448-456.
- [27] J. Zbontar, "fastMRI: An open dataset and benchmarks for accelerated MRI," 2018, arXiv:1811.08839. [Online]. Available: <https://arxiv.org/abs/1811.08839>
- [28] D. P. Kingma, J. Ba, "Adam: a method for stochastic optimization," in *Proc. 3rd Int. Conf. Learn. Represent. (ICLR)*, Y. Bengio and Y. LeCun, Eds. San Diego, CA, USA, May 2015. [Online]. Available: <https://arxiv.org/abs/1412.6980>
- [29] A. Krizhevsky, I. Sutskever, G. E. Hinton, "Imagenet classification with deep convolutional neural networks," *Advances in Neural Information Processing Systems, NIPS*, 2012, pp. 1097-1105.
- [30] Z. Wang, A. C. Bovik, H. R. Sheikh, E. P. Simoncelli, "Image quality assessment: from error visibility to structural similarity," *IEEE transactions on image processing.*, vol. 13, no. 4, pp. 600-612, 2004.
- [31] A. Beck and M. Teboulle, "A fast shrinkage-thresholding algorithm for linear inverse problems," *SIAM J. Imag. Sci.*, vol. 2, no. 1, pp. 183-202, 2009.